

NEW PHYSICAL INSIGHT ON THE CHANGES IN MAGNETIC TOPOLOGY DURING CORONAL MASS EJECTIONS: CASE STUDIES FOR THE 2002 APRIL 21 AND AUGUST 24 EVENTS

ILIA I. ROUSSEV,¹ NOÉ LUGAZ,¹ AND IGOR V. SOKOLOV²

Received 2007 July 11; accepted 2007 August 17; published 2007 September 28

ABSTRACT

In order to investigate the dynamics of the coronal mass ejections on 2002 April 21 and August 24, we performed a series of numerical simulations with an ad hoc driver for the eruptions. The resulting evolution of the solar corona for each event was followed by means of three-dimensional MHD simulations. We used *SOHO* MDI data to set realistic boundary conditions for the ambient magnetic field of the Sun. In our model, the loss of equilibrium of the coronal magnetic field and subsequent eruption were achieved by stretching the opposite polarity feet of a newly emerged magnetic dipole. The stressed magnetic field reconnects through null points and, in the case of the August 24 event, also through a quasi-separator. As a result, magnetic flux and helicity are transferred from the expanding flux system containing the evolving dipole to the nearby flux systems. Another result is the jumplike change in the location of one footprint of the erupting magnetic field. This Letter emphasizes the importance of studying CMEs on a case-by-case basis if we are to understand their dynamics, energetics, and interplanetary consequences.

Subject headings: acceleration of particles — MHD — shock waves — Sun: corona —
Sun: coronal mass ejections (CMEs) — Sun: magnetic fields

Online material: mpeg animation

1. INTRODUCTION

The physical causes of coronal mass ejections (CMEs) have been debated by the solar community for over three decades now (see a recent review by Rousev & Sokolov 2006). The vast majority of proposed models agrees that CMEs are the result of catastrophic loss of mechanical equilibrium or stability of the coronal magnetic field; it is argued that the magnetic field in the corona may contain sufficient energy in excess of the potential limit to power an eruption, provided that some critical state is reached.

The existing models typically involve idealized physical circumstances with either bipolar (Amari et al. 1999, 2003; Inhester et al. 1992; Rousev et al. 2003a) or quadrupolar (Antiochos et al. 1999; Syrovatskii 1982) underlying magnetic field geometries. The real Sun, however, demonstrates cases far more sophisticated than those studied in idealized configurations (Ugarte-Urra et al. 2007; Régnier & Priest 2007). Therefore, studying the actual magnetic field geometries involved during CMEs is crucial for understanding their energetics, dynamics, interplanetary (IP) consequences, etc. In a recent study, Rousev et al. (2004) included a realistic ambient magnetic field in simulating the dynamics of the CME event on 1998 May 2, and they succeeded in reproducing its general properties.

In this Letter, we present an improved methodology to model CMEs, which is applied to study the two very similar events of 2002 April 21 (CE1 hereafter) and 2002 August 24 (CE2 hereafter). CE1 took place on the west limb of the Sun, and it was associated with an X-class (X1.0) flare (Gallagher et al. 2002). The ejection originated from AR 9906, which was magnetically connected to the nearby AR 9902 and AR 9907. The CME drove a shock wave at a distance of $\sim 1.6\text{--}1.7 R_{\odot}$, as inferred from *SOHO* UVCS (Raymond et al. 2003), which traveled at a speed of $\sim 1500 \text{ km s}^{-1}$ (Gallagher et al. 2003).

CE1 took place near an open field region, which was magnetically connected to the Earth. A gradual solar energetic particle (SEP) event also occurred during April 21–23 in association with the shock dynamics in IP space (Tylka et al. 2005). The other event, CE2, which originated from AR 10069, was similar to CE1 in that (1) it also occurred on the west limb, (2) the source region was well connected to a number of nearby ARs (10067, 10068, and 10079), (3) there was an X3.1-class flare associated with the eruption, (4) a shock wave formed relatively close to the Sun and it traveled with comparable speed, and (5) a gradual SEP event occurred on August 24–25 in association with the eruption.

Note that for limb events, like those studied here, EUV and coronagraph white-light observations enable us to derive the acceleration profiles of the CMEs, as well as the structure of the ejecta and their shock waves (if formed). This, in turn, is not possible to be determined reliably for events occurring on the solar disk. Thus, the limb events provide better constraints for the invoked models of CME initiation and ambient solar wind conditions. For such events, however, it is generally difficult to infer from observations the surface dynamics of magnetic flux elements.

In this Letter, we compare CE1 and CE2 in terms of underlying magnetic geometry of the solar corona before and shortly after the CME onset. The study comprises fully three-dimensional (3D) compressible MHD simulations.

2. METHODOLOGY

2.1. Model of Steady-State Solar Corona and Solar Wind

In our numerical model, the steady-state solar corona and solar wind are constructed following the methodology of Rousev et al. (2003b). The initial condition for the coronal magnetic field is calculated by means of potential field extrapolation, following Altschuler et al. (1977), with a boundary condition for the radial magnetic field at the Sun, B_R , provided by *SOHO* MDI observations. In the field extrapolation, the source surface is set at $2.5 R_{\odot}$, and we use spherical harmonic coefficients

¹ Institute for Astronomy, University of Hawai'i, 2680 Woodlawn Drive, Honolulu, HI 96822; iroussev@ifa.hawaii.edu, nlugaz@ifa.hawaii.edu.

² Department of AOSS, University of Michigan, 2455 Hayward Street, Ann Arbor, MI 48109; igorsok@umich.edu.

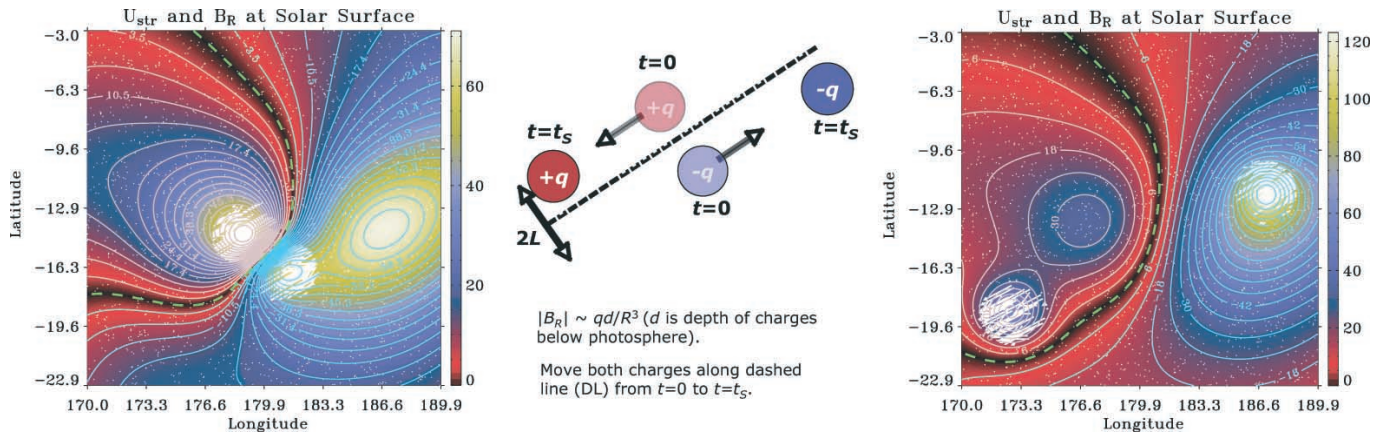


FIG. 1.—Zoomed-in magnetic maps of AR 9906 at $t = 0$ (left) and $t = t_s$ (right), and sketches of the initial and final configuration of the magnetic charges (middle). The maps show the strength of B_R in the vicinity of AR 9906 with superimposed magnetic field of the dipole. The polarity inversion line is shown as the dashed green line. The imposed velocity pattern resulting from the motion of the charges is shown as white short-dashed lines. The corresponding magnetic maps and charge geometry in the case of CE2 are not shown here, but they look qualitatively similar.

up to the order of 90. The high order of spherical harmonics used enables us to study ARs 9906 and 10069, and their neighbors, with high enough spatial resolution ($\sim 0.5'$). The “solar” boundary (SB) in our model is placed at a height of $0.1 R_\odot$ above the photosphere. This is adequate for our purposes, because in this study we are not interested in the thermodynamics of the solar plasma across the transition region. The choice of SB is also compatible with our empirical model of the solar wind, which originates from the low corona rather than the photosphere. We used *SOHO* MDI data taken 4 days prior to the events when the ARs were not so close to the limb. That is because it is difficult to derive B_R from photospheric measurements of the line-of-sight magnetic field as ARs approach the solar limb.

At the SB, in regions where the magnetic field strength B is greater than 18 G, the mass density ρ is enhanced in accordance with $\rho \propto B^2$, so that the Alfvén speed is limited to be no greater than $\sim 9000 \text{ km s}^{-1}$. Following Roussev et al. (2003b) the initially static corona with potential magnetic field is evolved to a new state with steady solar wind and nonpotential magnetic field.

The time-dependent MHD equations for a single compressible fluid are solved using the BATS-R-US code (Powell et al. 1999). The computations are performed in a rectangular box ($-20 \leq x \leq 20$, $-20 \leq y \leq 20$, $-20 \leq z \leq 20$) R_\odot , which consists of nonuniform Cartesian meshes. The grid is refined near the solar surface. Additional refinement is applied in the vicinity of the ARs of interest in order to better resolve the structure and dynamics of the solar plasma and coronal magnetic field therein. The total number of cells within the computational domain is of the order of 1.5×10^6 in both simulations: the smallest mesh size (at the SB) corresponds to $1.22 \times 10^{-3} R_\odot$, whereas the largest meshes have a size of $1.25 R_\odot$.

2.2. Solar Eruption Model

The new model to initiate CMEs presented here stems from a general consensus within the solar community (Su et al. 2007; Manchester 2007) that magnetic shear builds up as new ARs emerge on the solar surface. This process ultimately leads to the occurrence of CMEs, provided that the sheared coronal magnetic field becomes out of balance with the ambient mag-

netic field. Flux emergence in the form of dipolar magnetic field and moving magnetic features on the solar disk are often observed in connection with complex and dynamic ARs (Schrijver et al. 2005). For our events, *SOHO* MDI data show evidence of ongoing flux emergence in the ARs of interest (J. Li 2007, private communication). This evidence is more conclusive for CE1 than for CE2, since the latter showed a more complex dynamics of magnetic features on the solar surface. Motivated by these observations, here we simulate one consequence of flux emergence, namely shearing motions, on the overall evolution of the coronal field. However, we do not study the emergence process in a self-consistent manner. This is because our global model cannot be coupled to the upper convection zone through the photospheric boundary yet. Instead, we adopt an ad hoc approach for the shearing motions in the corona associated with flux emergence.

Here we model a newly emerged AR by the dipolar magnetic field of two point charges, $+q$ and $-q$ (see Fig. 1). The charges are separated initially by a distance $2L$ and are buried at a depth d below the SB, as in the model of Titov & Démoulin (1999). The chosen values for q , L , and d are $1.5 \times 10^{11} \text{ G km}^2$, $5 \times 10^3 \text{ km}$, and $3 \times 10^4 \text{ km}$, respectively. These parameters yield a peak value for the radial magnetic field at the SB of the order of 47 G.

The magnetic field produced by the two charges is superimposed onto the extrapolated potential magnetic field constrained by *SOHO* MDI data. The resulting coronal magnetic field comprises the new initial condition, which is still potential everywhere. This is then evolved with BATS-R-US to a new nonpotential magnetic configuration with steady-state solar wind, as described above. Once the steady-state is reached at $t = 0$, the two magnetic charges are moved apart quasi-steadily in the way illustrated in Figure 1 up to $t = t_s = 25$ minutes. The speed of the charges increases linearly for $0 < t \leq t_s/3$, and then it is maintained at a constant level of about 100 km s^{-1} up to $t = t_s$; the charge motion stops at $t = t_s$. Note here that the speed of charge separation is at most a few percent ($\leq 2\%$) of the local Alfvén speed. In addition to imposing a localized horizontal flow at the SB, the radial component of the dipole field at the boundary is also updated in a time-dependent fashion to reflect the new position of the charges. As the result of moving $+q$ and $-q$ apart, the magnetic field lines connecting

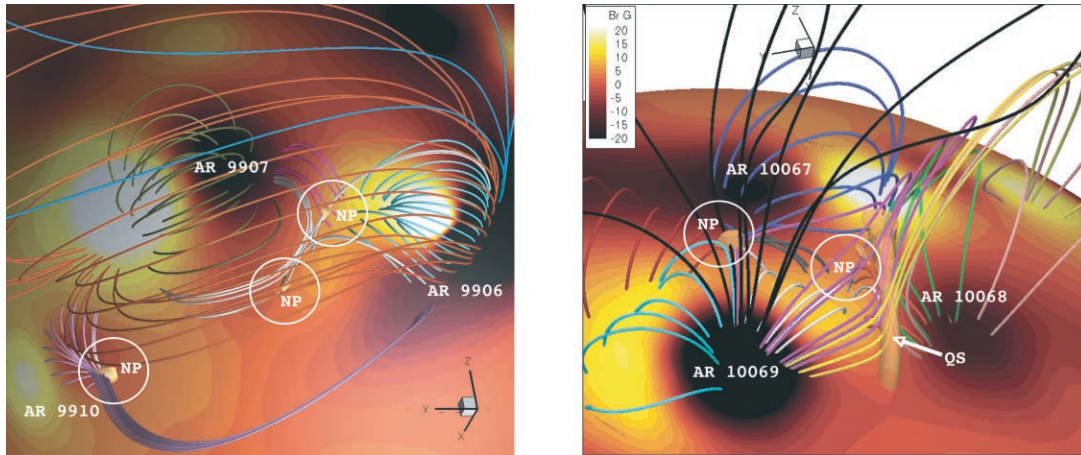


FIG. 2.—Magnetic topologies for CE1 (*left*) and CE2 at $t = 0$. The background color in each image shows B_r at the SB; the magnetic field is a superposition of the potential field extrapolated from *SOHO* MDI data and that of the dipole. The ARs of interest are annotated as shown. The colored lines are 3D magnetic field lines, where each color represents a distinct flux system. The blue (black) field lines in the left (right) image are open in IP space. The magnetic null points (NPs) in the corona are encircled. In the case of CE2, there is a quasi-separator (QS) extending from a local minimum of \mathbf{B} at the solar surface through a NP higher up in the corona (between the three ARs shown). We used the plasma- β as a proxy to visualize the NPs and QS, which are shown here as isosurfaces of $\beta = 0.2$ and $\beta = 0.1$, respectively.

the two spots of the dipole are stretched and twisted. (The maximum amount of magnetic shear achieved along the polarity inversion line is less than $\pi/2$.) Thus, the magnetic energy and helicity of the dipole field gradually increase over time, which is what is required to power an eruption. Also subject to change is the mutual helicity of the evolving dipole field with respect to the surrounding magnetic field of nearby flux systems.

3. DISCUSSION OF CORONAL TOPOLOGY AND EVOLUTION

With appropriate choice of parameters describing the relative position of the charges and their strength and speed of motion, the system can evolve through a sequence of quasi-equilibrium states toward a point where the stability breaks down. Then, the “energized” magnetic field of the dipole is no longer confined by the overlying field and it erupts, manifesting a CME. After carefully choosing the model parameters, one can achieve CMEs that closely resemble observed events, as is accomplished here for CE1 and CE2. The derived CME acceleration profiles and simulated coronagraphic images of Thomson scattered light are found in good agreement with relevant observations.

The relevant magnetic topology for each event at $t = 0$ is shown in Figure 2. This reveals that the coronal magnetic field for both events is sufficiently complex, showing a number of null points (NPs; three or more), a quasi-separator (QS; in the case of CE2), and a number of distinct magnetic flux systems (as many as 10 for CE2, as shown). Here we only show the topological features which we believe played a role during the CME events. There are regions of open magnetic flux in the vicinity of both AR 9906 (blue field lines in left panel of Fig. 2) and AR 10069 (black field lines in the right panel). However, in the case of AR 9906, the open flux overlays one of the NPs, whereas in the case of AR 10069 two of the NPs and the QS reside within regions of closed loops. This finding might be one prerequisite that explains the difference discussed by Tylka et al. (2005) between the two SEP events.

At $t = 0$, the evolution of the small-scale dipole commences, and the magnetic configuration is gradually driven toward loss of stability. In this process, electric currents start to build at

the NPs and QS since the pressure balance there is perturbed. As the $+q$ and $-q$ charges move apart, an electric current is generated, which flows along the loops connecting the moving spots of opposite magnetic polarity. As a result, the magnetic energy of the evolving dipole monotonically increases in time, and the loops connecting the two moving spots gradually expand. The excess magnetic energy that is built in the sheared field prior to the onset of reconnection is 2.01×10^{32} ergs in the case of CE1 and 2.13×10^{32} ergs in the case of CE2.

As the sheared field expands, it starts to reconnect with the magnetic field from the neighboring flux systems (see Fig. 2) through the preexisting NPs and QS (in the case of CE2). This reconnection removes the overlying field sideways (thus it no longer has confining effect on the eruption) as in the “breakout model” of Antiochos et al. (1999). Once the “magnetic breakout” sets in at $t = 18$ minutes ($t = 16$ minutes) in the case of CE1 (CE2), the free energy stored in the sheared coronal field starts being converted into kinetic energy of bulk plasma motions and heat. In the case of CE1 (CE2), as much as 17% (15%) of the excess magnetic energy built in the field prior to the onset of “breakout reconnection” is ultimately converted into kinetic energy, and roughly 12% (14%) of it goes into heat; 95% of the energy conversion occurs within 14 minutes (11 minutes) of the onset of “breakout reconnection” in the case of CE1 (CE2). For both events, approximately 3×10^{15} g of solar plasma is ejected into outer space.

In the more sophisticated magnetic topologies studied here, reconnection via NPs nearby, but sideways of the expanding field, serves to change the connectivity of the erupting field; i.e., it causes jumplike changes in the CME footprint(s), which is not a feature of the classical breakout model. Thus, what is seen in our simulations is a generalization of this CME scenario. We find that the footprint separation increases in time and the mutual helicity of the flux systems undergoing reconnection transforms into self-helicity. Also, in the case of CE2, the QS (see discussion in Titov et al. 2002) evolves into a current sheet above the expanding current loop. Fast reconnection in this sheet enables rapid acceleration of the current loop.

Here we emphasize that the erupting field is found to be a mixture of magnetic elements from various flux systems. This

is valid for both events studied here, and we believe that the majority of CMEs originating from complex ARs undergo similar evolution. Figure 3 illustrates the erupting magnetic flux rope in the case of CE1.

4. CONCLUSIONS

In a recent study, Ugarte-Urra et al. (2007) found that (1) 7 out of 26 CMEs can be interpreted with the breakout model of Antiochos et al. (1999), (2) 12 events can be explained with other CME models (in dipolar geometries), and (3) 7 events remain unclassifiable. This implies that $\sim 27\%$ of observed CMEs are more sophisticated than those modeled in idealized magnetic geometries (bipolar or quadrupolar). It also proves necessary to study CMEs on a case-by-case basis if we are to understand their energetics, dynamics, etc., which was our approach undertaken here. By means of 3D compressible MHD simulations, we were able to determine that multiple NPs in the corona (three or more) and a quasi-separator (in the case of CE2) played a role during the two complex CMEs modeled here.

Our MHD simulations showed that the dynamic reconstruction of the erupting magnetic field due to reconnection has one important consequence; that is, the location of one footprint (in reality maybe both) of the erupting magnetic field changes in time in a jumplike manner. This may have some implications for the production of SEPs in terms of varying seed population. Solar researchers often assume that the footprints of CMEs remain fixed at the Sun. This is because the vast majority of CME models to date (see discussion in Roussev & Sokolov 2006) involve idealized ambient magnetic fields, which makes it difficult to investigate effects such as this. Here we argue that this is not generally true, and that the preexisting magnetic topology determines to a large extent how the erupting magnetic field will evolve. That is why it is imperative to study CMEs on a case-by-case basis. We also argue that due to the topological reconstruction of the erupting magnetic field, the energy constraint for field opening imposed by the Aly-Sturrock theorem (see discussion in Forbes 2000) may not hold true for complex events such as CE1 and CE2. This may be

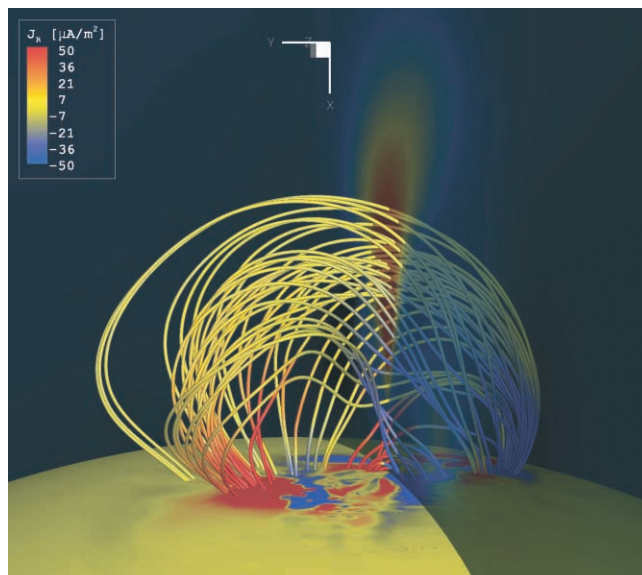


FIG. 3.—Three-dimensional structure of the stressed field lines of the evolving magnetic dipole in the case of CE1 at $t = t_s$. The color code along the field lines visualizes the radial component of the current density, J_r . The radial velocity of the erupting magnetic field is shown on a translucent plane cutting through the middle of the flux rope; the red (yellow) color corresponds to a flow velocity of the order of 1000 km s^{-1} (700 km s^{-1}). The SB is shown as the yellow sphere. The flux rope in the case of CE2 looks qualitatively similar. [This figure is available as an mpeg animation in the electronic edition of the Journal.]

the key to explain fast ejections on the Sun, but it remains to be proven.

The authors wish to thank Jen Harper and an unknown referee for the useful comments made on the manuscript. We are grateful to Yang Liu and Jing Li for providing us with the desired *SOHO* MDI data. This research work was supported by NSF grants ATM 04-54469 (FDSS), ATM 06-31790 (SHINE), and ATM 06-39335 (CAREER), as well as NASA-LWS grants NNG05GM70G and NNX07AC13G.

REFERENCES

- Altschuler, M. D., Levine, R. H., Stix, M., & Harvey, J. 1977, *Sol. Phys.*, 51, 345
- Amari, T., Luciani, J. F., Mikić, Z., & Linker, J. 1999, *ApJ*, 518, L57
- Amari, T., et al. 2003, *ApJ*, 585, 1073
- Antiochos, S. K., DeVore, C. R., & Klimchuk, J. A. 1999, *ApJ*, 510, 485
- Forbes, T. G. 2000, *J. Geophys. Res.*, 105, 23153
- Gallagher, P. T., Dennis, B. R., Krucker, S., Schwartz, R. A., & Tolbert, A. K. 2002, *Sol. Phys.*, 210, 341
- Gallagher, P. T., Lawrence, G. R., & Dennis, B. R. 2003, *ApJ*, 588, L53
- Inhester, B., Birn, J., & Hesse, M. 1992, *Sol. Phys.*, 138, 257
- Manchester, W. B., IV. 2007, *ApJ*, 666, 532
- Powell, K. G., et al. 1999, *J. Comput. Phys.*, 154, 284
- Raymond, J. C., Ciaravella, A., Dobrzycka, D., Strachan, L., Ko, Y.-K., Uzzo, M., & Raouafi, N.-E. 2003, *ApJ*, 597, 1106
- Régnier, S., & Priest, E. R. 2007, *A&A*, 468, 701
- Roussev, I. I., & Sokolov, I. V. 2006, in *Solar Eruptions and Energetic Particles*, ed. N. Gopalswamy, R. Mewaldt, & J. Torsti (Geophys. Monogr. 165; Washington: AGU), 89
- Roussev, I. I., et al. 2003a, *ApJ*, 588, L45
- . 2003b, *ApJ*, 595, L57
- . 2004, *ApJ*, 605, L73
- Schrijver, C. J., DeRosa, M. L., Title, A. M., & Metcalf, T. R. 2005, *ApJ*, 628, 501
- Su, Y., Golub, L., & Van Ballegooijen, A. A. 2007, *ApJ*, 655, 606
- Syrovatskii, S. I. 1982, *Sol. Phys.*, 76, 3
- Titov, V. S., & Démoulin, P. 1999, *A&A*, 351, 707
- Titov, V. S., Hornig, G., & Démoulin, P. 2002, *J. Geophys. Res.*, 107, 1164
- Tylka, A. J., et al. 2005, *ApJ*, 625, 474
- Ugarte-Urra, I., Warren, H. P., & Winebarger, A. R. 2007, *ApJ*, 662, 1293